Sea ice pCO_2 dynamics and air-ice CO_2 fluxes during the SIMBA Experiment – Bellingshausen Sea, Antarctica

Geilfus N.-X.[1,2,3], Tison J.-L.[2], Ackley S.F.[4], Galley R.J.[5], Rysgaard S.[1,5,6] , Miller L.A.[7] and Delille B.[3]

[1] Arctic Research Centre, Aarhus University, Aarhus, Denmark

[2] Laboratoire de Glaciologie, Université Libre de Bruxelles, Bruxelles, Belgium

[3] Unité d'Océanographie Chimique, Université de Liège, Liège, Belgium

[4] Department of Geological Sciences, University of Texas at San Antonio, San Antonio, TX, USA

[5] Centre for Earth Observation Science, University of Manitoba, Winnipeg, Canada

[6] Greenland Climate Research Centre, Greenland Institute of Natural Resources, Nuuk, Greenland

[7] Centre for Ocean Climate Chemistry, Institute of Ocean Sciences, Fisheries and Oceans, Canada, Sidney, BC, Canada.

Keywords: sea ice, snow, CO_2, Antarctic, CO_2 fluxes

1. Abstract

Temporal evolution of pCO_2 profiles in sea ice in the Bellingshausen Sea, Antarctica, in October 2007 shows physical and thermodynamic processes controls the CO_2 system in the ice. During the survey, cyclical warming and cooling strongly influenced the physical, chemical and thermodynamic properties of the ice cover. Two sampling sites with contrasting characteristics of ice and snow thickness were sampled: one had little snow accumulation (from 8 to 25 cm) and larger temperature and salinity variations than the second site, where the snow cover was up to 38 cm thick and therefore better insulated the underlying sea ice. We show that each cooling/warming event was associated with an increase/decrease in the brine salinity, total alkalinity (TA), total dissolved inorganic carbon (TCO_2), and *in situ* brine and bulk ice CO_2 partial pressures (pCO_2). Thicker snow covers reduced the amplitude of these changes: snow cover influences the sea ice carbonate system by modulating the temperature and therefore the salinity of the sea ice cover. Results indicate that pCO_2 was undersaturated with respect to the atmosphere both in the *in situ* bulk ice (from 10 to 193 µatm), and brine (from 65 to 293 µatm), causing the sea ice to act as a sink for atmospheric CO_2 (up to 2.9 mmol m^{-2} d^{-1}), despite supersaturation of the underlying seawater (up to 462 µatm).

2. Introduction

Sea ice formation and melting may have a strong impact on the carbon cycle of polar oceans [e.g., *Rysgaard et al.,* 2011, *Delille et al.,* 2014]. However, processes related to freezing and melting of sea ice, as well as their impact on CO_2 exchanges with the atmosphere, are still poorly understood [*Parmentier et al.,* 2013]. Detailed studies have been conducted on sea ice inorganic carbon chemistry and the impact of sea ice on the carbon cycle and the CO_2 exchanges between atmosphere, sea ice, and the ocean over the last decade [*Semiletov et al.,* 2004; *Zemmelink et al.,* 2006; *Rysgaard et al.,* 2007; 2011; 2012; *Delille et al.,* 2007; 2014; *Miller et al.,* 2011, *Papakyriakou and Miller* 2011; *Geilfus et al.,* 2012a; 2013; *Nomura et al.,* 2010a; 2013]. These studies have shown that in both hemispheres, CO_2-carbonate chemistry in sea ice and brine is heterogeneous and variable, resulting in complex CO_2 dynamics.

The CO_2 chemistry of sea ice seems to be highly dependent on brine salinity, which is controlled by ice temperature [*Weeks,* 2010]. Both brine concentration during ice growth and brine dilution during ice melt play major roles in the carbonate system dynamics within sea ice [*Papadimitriou et al.,* 2004; *Nomura et al.,* 2010a; *Geilfus et al.,* 2012a]. In parallel, temperature dependence of both the dissociation constants of the carbonate system and the Henry's Law constant for CO_2 affect pCO_2 in sea ice. Brine concentration/dilution can be associated with precipitation/dissolution of calcium carbonate within the sea ice, also promoting an increase/decrease in the *in situ* brine pCO_2 [*Papadimitriou et al.,* 2004; 2008; *Rysgaard et al.,* 2007; 2012; 2013; *Geilfus et al.,* 2012a; 2013]. Primary production

and respiration can also affect the CO_2-carbonate system within sea ice [*Thomas and Dieckmann* 2010; *Dieckmann and Hellmer,* 2010; Delille et al., 2007]. Finally, brine and gas transport within sea ice and across the air–ice and ice–water interfaces affect TA, TCO_2, and CO_2 distributions within the ice, together with the overall amount of CO_2 in the sea ice. The role of ice-covered oceans in the CO_2 balance has been largely ignored because continuous sea ice cover is assumed to impede gaseous exchange with the atmosphere. However, recent studies show that sea ice may mediate the air to sea CO_2 transfer. Understanding of the seasonal and geographical conditions of the inorganic carbon dynamics related with sea ice is limited. The main goal of this study is to add to the still limited database on inorganic carbon dynamic in ice-covered seas.

Although snow thickness and distribution are variable and primarily result from wind-induced redistribution during storms [*Weeks* 2010], the impact of snow cover on the thermal evolution of sea ice can be significant [*Massom et al.,* 2001]. Snow, which has a low thermal conductivity compared to sea ice [*Massom et al.,* 2001], provides thermal insulation between the cold air and the ice. The presence of a thick snow cover also affects the isostatic balance, potentially resulting in negative freeboard (i.e. the snow–ice interface is submerged below the seawater level). If the sea ice is permeable throughout the entire ice column, negative freeboard causes vertical flooding to at least the snow-ice interface through open brine channels. The percolation threshold above which columnar sea ice is considered permeable to fluid transport corresponds to a brine volume (which is controlled by temperature and salinity) of 5% [*Golden et al.,* 1998; 2007].

Therefore, snow accumulation could impact the CO_2-carbonate system within sea ice by regulating the ice temperature and the extent of flooding. The impact of snow on the CO_2 exchanges between sea ice and the atmosphere has previously been discussed by *Nomura et al.,* [2010b]; these authors suggested that a snow cover thicker than 9 cm could prevent any sea ice-atmosphere exchanges of CO_2 and that melting snow can act as a physical barrier to CO_2 fluxes.

In this study, we examine the temporal evolution of *in situ* brine and bulk ice pCO_2 profiles associated with physical and biogeochemical variables in the sea ice cover of two contrasting study sites, named "Brussels" and "Liège" between 1 and 23 October 2007, during the Sea Ice Mass Balance in Antarctic (SIMBA) cruise (Bellingshausen Sea, Antarctica) (Figure 1) [*Lewis et al.,* 2011]. Further, we differentiate the dynamics of *in situ* brine and bulk ice pCO_2. Sea ice temperature and bulk salinity differences at these two stations, in part due to substantial difference in snow cover, impact the inorganic carbon dynamics within sea ice and its brine and the related air–ice CO_2 fluxes.

3. Study site, materials and methods

a. Selection of study site

The Sea Ice Mass Balance in the Antarctic (SIMBA) cruise investigated the physical and biological interactions between the ocean, sea ice, snow cover and atmosphere in the Bellingshausen Sea, onboard the RV *Nathaniel B. Palmer* (NBP) in October 2007. During this ~ one-month experiment, the vessel was moored to a first year sea-ice floe, the Ice Station Belgica (ISB), south of Peter I Island, at approximately 69-71°S and 90-95°W (Figure 1). The station was chosen for its wide

106 variety of ice types and snow cover [*Lewis et al.,* 2011], characteristic of the greater
107 region and the size of the ice floe (~ 5 km^2) was deemed large enough to survive the
108 duration of the field experiment. Sampling was conducted at two distinct sites based
109 on: (i) homogeneity of the surface properties within each site, to reduce within-site
110 spatial variability; (ii) the contrast in ice and snow properties between the two
111 chosen sites; and (iii) maximum distance from the ship (0.8 km and 1.1 km), to
112 prevent sample contamination. Each site was 100x60 m and subdivided into small
113 work sub-areas approximately 5m x 5m. The 25 m^2 sub-areas were located adjacent
114 to each other to minimize spatial variability [*Lewis et al.,* 2011]. Each station was
115 sampled at 5-day intervals: the Brussels site (low snow cover, at 0.8 km) was
116 sampled on 1, 6, 11, 16, and 21 October and the Liège site (high snow cover, at 1.1
117 km) was sampled on 3, 8, 13, 18, and 23 October (Figure 2).

118 **b. Sampling procedures**

119 Ice cores were collected using an electro-polished stainless steel corer using an
120 electric drill head, connected by a long cord to a power supply generator located
121 downwind. Cores were immediately wrapped in polyethylene bags and placed in an
122 insulated box filled with gel packs pre-cooled to -30°C in order to limit brine
123 drainage from samples [*Tison et al.,* 2008] and brought back to the ship laboratory.
124 Sackholes [*Gleitz et al.,* 1995] for collecting brine were drilled to four depths: 15, 30,
125 40, and 50 cm at the Brussels site; and 15, 30, 60 and 90 cm at the Liège site. Each
126 sackhole was covered with a plastic lid to prevent contamination by falling snow.
127 Brine seeped into the sackholes for 10 to 60 min before collection using a peristaltic
128 pump (Cole Palmer, Masterflex-Environmental Sampler). Under-ice seawater was

collected using the same peristaltic pump, with the inlet positioned at the ice–water interface, and at 1 and 30 m depths. On each sampling date, ice cores, brine and seawater were collected and analyzed for a full range of physical and biogeochemical variables: temperature (T), salinity (S), water stable isotopes of $\delta^{18}O$, chlorophyll *a* (Chl *a*), total alkalinity (TA), pH_T, and *in situ* CO_2 partial pressure (pCO_2). Brine samples for pH_T and TA analyses were only collected from the shallowest sackhole depth (at 0 to 15 cm) and at 0 to 40 cm depth at the Brussels site and 0 to 60 cm depth at the Liège site sackholes.

c. Materials and methods

The ice temperature was measured immediately after extraction of the ice core using a calibrated temperature probe (TESTO 720, ± 0.1°C precision) inserted into pre-drilled holes (~ 5 cm intervals) perpendicular to the core sides. In the field, the ice core dedicated to bulk ice salinity measurements was cut into 5 cm thick slices which were stored in separate, closed containers. These ice samples were melted at room temperature on board and bulk ice salinity on the practical salinity scale was determined from conductivity and temperature using a portable calibrated Orion 3-Star conductivity meter (precision of ±0.1). Samples with salinity higher than 42 were diluted with ultrapure water using an analytical balance. Brine volumes profiles were calculated for each core using these bulk ice salinities and ice temperatures according to *Cox and Weeks* [1983] for ice temperatures below -2°C and according to *Leppäranta and Manninen* [1988] for ice temperatures within the range -2°C to 0°C. Calculated brine salinity profiles were determined from the *in situ* ice temperatures (after *Cox and Weeks* [1983]).

Aliquots (10 ml) of the bulk melted sea ice samples were transferred to gas tight vials for $\delta^{18}O$ measurements at the Australian Antarctic CRC. Isotope ratios were measured with a dual-inlet VG SIRA mass spectrometer using the conventional water-CO_2 equilibration method (accuracy with respect to VSMOW = ± 0.12 ‰).

The pH of the sea-ice brine and seawater was measured using a Metrohm combined electrode calibrated on the total hydrogen ion scale (pH_T) using TRIS (2-amino-2-hydroxymethyl-1.3-propanediol) and AMP (2-aminopyridine) buffers prepared at salinities of 35 and 75 according to the formulations proposed by *DOE* [1994]. Samples were maintained as close as possible to their in situ temperature (typically below 3°C), and measurements of pH_T were carried out as soon as possible after upon return to the ship laboratory (typically less than 2 hours after sampling). The pH electrode was calibrated at temperatures ranging from 0 to 4°C and at salinities ranging from 35 to 75. The accuracy of the pH_T measurements was ±0.01 pH unit [*Frankignoulle and Borges,* 2001].

Total alkalinity in the brine and underlying seawater was measured by open-cell titration with HCl 0.1M, and the endpoints were determined according to *Gran* [1952]. Routine analyses of Certified Reference Materials provided by A. G. Dickson, Scripps Institution of Oceanography, verified that the error in these TA data was smaller than ± 4 μmol kg^{-1}. Total inorganic carbon (TCO_2) and pCO_2 (denoted as pCO_{2calc}) were calculated from TA and pH_T using the CO_2 acidity constants of *Mehrbach et al.,* [1973] refit by *Dickson and Millero* [1987] and other constants advocated by *DOE* [1994]. We assumed that the CO_2 dissociation constants were

174 applicable at subzero temperatures as suggested by *Marion* [2001] and *Delille et al.,*
175 [2007].

176 Brine and underlying seawater pCO_2 were measured *in situ* using a custom-made
177 equilibration system [*Geilfus et al.,* 2012a]. The system consisted of a membrane
178 contactor equilibrator (Membrana, Liqui-cell) connected to a non-dispersive infrared
179 gas analyzer (IRGA, Li-Cor 6262) via a closed air loop. Brine and airflow rates from
180 the equilibrator and IRGA were approximately 2 L min^{-1} and 3 L min^{-1}respectively.
181 Temperature was measured within the sackholes or under-ice water and at the
182 equilibrator outlet simultaneously using Li-Cor temperature sensors. The pCO_2
183 values were temperature-corrected assuming that the *Copin Montégut* [1988]
184 relation is valid at low temperatures and high salinities. The IRGA was calibrated
185 immediately upon returning to the ship while the analyzer was still cold. All devices,
186 except the peristaltic pump, were enclosed in an insulated box that contained a 12 V
187 power source providing enough heat to keep the inside temperature just above 0°C.

188 Ice cores were kept frozen during storage and shipping for subsequent analysis
189 of bulk ice pCO_2 at the Laboratoire de Glaciologie, Université Libre de Bruxelles,
190 Belgium. The general principle of the method was to equilibrate the sea ice samples
191 at the *in situ* temperature with a mixture of N_2 and CO_2 at known concentrations (so-
192 called standard gas, 396 µatm) and rapidly extract the gas into a Varian 3300 gas
193 chromatograph under vacuum [*Geilfus et al.,* 2012b]. Each ice sample was cut into a 4
194 x 4 x 4.5 cm cube to tightly fit the equilibration container, thereby both minimizing
195 the headspace and keeping it consistent. The standard gas was injected at 1013 mbar
196 into the equilibration container containing the ice sample. Then the container with

197 the ice sample is placed in a thermostatic bath setup at the field *in situ* temperature
198 for 24 hours. This timing is chosen to ensure that the sample is re-equilibrated to the
199 brine volume and chemical conditions at the *in situ* temperature. A quick injection
200 into the gas chromatograph then allows the reconstruction of the equilibrium brine
201 pCO_2 at the *in situ* temperature.

202

203 This method is only valid if the ice is permeable at the *in situ* conditions [*Geilfus*
204 *et al.,* 2012b].

205 Air–ice CO_2 fluxes were measured using an accumulation chamber (West
206 System) placed on top of the ice. The chamber was a metal cylinder closed at the top,
207 with an internal diameter of 20 cm and an internal height of 9.7 cm. A rubber seal
208 surrounded by a serrated steel edge ensured an airtight connection between the ice
209 and the chamber. Over snow, a steel tube was mounted at the base of the chamber to
210 enclose the snowpack to the ice surface and prevent lateral infiltration of air into the
211 chambered volume of snow. The chamber was connected in a closed loop to the IRGA
212 with an air pump rate of 3 L min^{-1}. The pCO_2 in the chamber was recorded every 30
213 sec for a minimum of 5 min. The flux was computed from the slope of the linear
214 regression of pCO_2 versus time (r^2>0.99) according to *Frankignoulle* [1988], taking
215 into account the volume of ice or snow enclosed within the chamber. The average
216 uncertainty of the flux computation due to the standard error of the regression slope
217 was ±3%.

218 ## 4. Results

a. Atmospheric conditions

During the 2007 winter–spring transition in the Bellingshausen Sea, several low-pressure systems of varying intensity and length occurred at the sampling location. Fluctuations in the air temperature are shown in Figure 3, along with the surface ice temperature measured at each station. At least three successive cycles of warming and cooling were recorded with air temperatures ranging from 0.5°C to -20°C. These cycles consisted of warm atmospheric fronts from the north, generally accompanied by high velocity winds and precipitation, followed by cold air temperatures and little precipitation [*Lewis et al.,* 2011; *Vancoppenolle et al.,* 2011].

b. Sea ice and snow conditions

The Brussels and Liège sites had contrasting conditions in snow, ice thickness (Figure 2) and ice texture, which are presented in detail by *Lewis et al.,* [2011].

At the Brussels site, the ice thickness, as determined by coring, ranged from 55 to 67 cm, while the snow cover ranged from 8 to 25 cm (Figure 2a). The ice freeboard was positive and ranged from 0.7 to 3 cm. The ice cover was mainly composed of columnar crystals [*Lewis et al.,* 2011]. The ice temperatures ranged from -1.5 to -6.1°C (Figure 4). The main changes in temperatures were observed in the top 40 cm of the ice cover, oscillating between cooling and warming events within a 1°C temperature window (from -3°C to -4°C), except on 16 October, when the near-surface ice temperature decreased to -6.1°C and the top 40 cm reached it's minimum observed temperature. The bulk ice salinity ranged from 3.4 to 14.1. The profiles were typically S-shaped, as described by *Eicken* [1992], with higher salinities

241 (from 11.5 to 14.1) in the top layer, dropping to minimum values (on average, S =
242 4.1) at the bottom. Between 1 and 16 October, the brine salinities increased from the
243 bottom to the top of the ice cover, with values close to seawater (S=34) at the bottom
244 to a maximum of 101 at the top on 16 October. The brine volume was always greater
245 than 5%, except in the top 20 cm of the ice cover on 16 October. The $\delta^{18}O$ isotopic
246 ratio ranged from -5.8 ‰ to 2.1 ‰. The top 15 cm showed negative $\delta^{18}O$ values at
247 each sample interval, while the rest of the profile was increasing steadily towards a
248 value of +2 ‰ at the bottom.

249 At the Liège site, the ice and snow cover were thicker than at the Brussels site
250 and ranged from 99 to 106 cm and from 28 to 38 cm, respectively (Figure 2b). The
251 ice freeboard was negative on 18 and 23 October, flooding the snow–ice interface.
252 The ice cover at the Liège site was mainly composed of granular sea ice with
253 inclusions of columnar and snow ice layers at different levels in the ice profile (see
254 *Lewis et al.,* [2011] for a detailed description of the ice texture profile at the Liège
255 site). These inclusions, associated with sharp excursions in the $\delta^{18}O$ ratios (Figure 4),
256 indicate a history of dynamic conditions and repeated subsequent rafting events
257 [*Lewis et al.,* 2011]. The observed variations of the bulk ice temperature and salinity,
258 as well as the calculated brine salinity, were smaller than those observed at Brussels
259 (Figure 4). The ice temperature ranged from -1.3°C to -3.7°C. The ice cover showed
260 similar warm and isothermal profiles on 3, 8 and 23 October, with brine salinities
261 close to seawater values throughout the ice column. The ice cover cooled from 8 to
262 18 October, when the minimum temperature and maximum brine salinity were
263 observed, as we also observed at the Brussels site. The bulk ice salinity ranged from

2.3 to 13.8, and the salinity profiles were also typically S-shaped, with the top layer ranging from 6.5 to 13.8, while the average salinity of the bottom layer was 3. The calculated brine volume fraction was always above 5%. The $\delta^{18}O$ ratios ranged from -4.9 ‰ to 2.9 ‰. At the top of the ice, $\delta^{18}O$ was negative from 3 to 13 October and positive on our last two sampling days. In the lower half of the profiles, $\delta^{18}O$ values were generally around 1‰, although the cores sampled on 18 and 23 October had negative $\delta^{18}O$ intervals, further indicative of ice rafting.

c. Carbonate system

At the Brussels site, TA in brine sampled from sackholes ranged from 2406 to 4855 µmol kg^{-1} while TCO_2 ranged from 2288 to 4110 µmol kg^{-1} (Figure 5). Changes in TA and TCO_2 closely mimicked the salinity changes. Normalizing TA and TCO_2 to a salinity of 34 (denoted as nTA and $nTCO_2$) indicate the sensitivity of these parameters to salinity changes; both nTA and $nTCO_2$ remain relatively stable (2350 µmol kg^{-1} and 2010 µmol kg^{-1} respectively). The pH_T ranged from 7.9 to 8.8 and increased continuously during the survey, except for a significant decrease in the deeper brine on 16 October (Figure 5) associated with decreased brine salinity and TA. The *in situ* brine pCO_2 ranged from 82 to 392 µatm. Brine was undersaturated in CO_2 relative to the atmosphere (383.8 µatm in 2007), except on 16 October (Figure 5, 6). The brine pCO_{2calc} was similar to brine pCO_2 measured *in situ* (± 50 µatm), except on 1 October when brine pCO_{2calc} was extremely high (620 µatm, Figure 5). From 1 to 6 October, the *in situ* brine pCO_2 values were from 210 to 271 µatm (Figure 6). Then, the *in situ* brine pCO_2 decreased on 11 October and increased again on 16 October to concentrations ranging from 248 to 392 µatm. On 21 October, the *in situ*

287 brine pCO_2 decreased down to concentrations ranging from 82 to 115 µatm. The bulk
288 ice pCO_2 ranged from 15 to 150 µatm (Figure 6), generally increasing with depth and
289 lower or equal to the brine pCO_2.

290 At the Liège site, the brine salinity ranged from 38.1 to 58.3. TA ranged from
291 2806 to 4074 µmol kg^{-1} while TCO_2 ranged from 1826 to 3590 µmol kg^{-1} (Figure 5).
292 As for the Brussels site, TA and TCO_2 changes seem closely related to salinity
293 changes, except on 3 October. The pH_T ranged from 8.5 to 8.7 with a significant
294 increase on 13 October to a maximum of 9.2 (Figure 5). The *in situ* brine pCO_2 was
295 undersaturated compared to the atmosphere, with values ranging from 65 to 183
296 µatm. These values were consistent with the brine pCO_{2calc} (± 80 µatm) Changes of
297 the *in situ* brine pCO_2 were smaller than the variations at the Brussels site. The most
298 significant change occurred on 18 October where the *in situ* brine pCO_2 increased to
299 concentrations ranging from 147 to 183 µatm. The bulk ice pCO_2 ranged from 9 to
300 193 µatm (Figure 6). Bulk ice pCO_2 were here generally more consistent with brine
301 pCO_2, except in the colder 8 and 18 October stations. The minimum concentrations
302 were observed in the top 20 cm of the ice cover while the maximum concentrations
303 were observed at the sea ice interface with the underlying seawater. The mean bulk
304 ice pCO_2 ranged from 70 to 79 µatm from 3 to 18 October and increased to 97 µatm
305 on 23 October.

306 The salinity and CO_2 system parameters were relatively constant in the
307 underlying seawater during our survey (Figure 7). We observed a slight decrease in
308 the salinity on 13 October, while pH_T decreased and TCO_2 increased on 11 and 13

October. The seawater pCO_2 measured *in situ* was supersaturated relative to the atmosphere, ranging from 401 to 462 µatm.

d. Air-ice CO_2 fluxes

The CO_2 fluxes measured at the sea ice and snow interfaces with the atmosphere suggest that, except for a small efflux of 0.3 mmol m^{-2} d^{-1} measured over the ice at the Brussels site on 16 October, both the sea ice and the snow acted as sinks for atmospheric CO_2 during our study (Figure 8). In general, Brussels sea ice showed a small uptake of atmospheric CO_2 that was not significantly different from zero (Figure 8a). At Liège, the uptake of atmospheric CO_2 was more substantial, ranging up to -2.9 mmol m^{-2} d^{-1} over sea ice with smaller values over snow covered ice (Figure 8b).

5. Discussion

a. Impact of atmospheric forcing and snow thickness on the physical properties of the ice cover

At the beginning of the sampling period the ice cover at stations Brussels and Liège were nearly isothermal. Subsequently, successive warm and cold events associated with passing atmospheric fronts (Figure 3) affected the temperature gradient within the ice cover significantly. At both sites, the fluctuations in ice temperature occurred mainly in the top 40 cm (Figure 4). The high brine salinities associated with the cold ice temperature at the top of the ice resulted in an unstable salinity gradient within the ice cover (Figure 4). This may have initiated overturning of brine and the mixing with underlying seawater with brine moving downward through the ice cover to be

331 replaced by underlying seawater moving upward [*Lewis et al.,* 2011]. To confirm this
332 hypothesis, *Lewis et al.,* [2011] reported presence of dissolution features observed
333 on freshly extracted ice cores and thick sections as well as under-ice photographs
334 clearly showing brine drainage at the ice bottom. In addition, analysis of the Rayleigh
335 numbers (Ra) provided by *Brabant* [2012] suggests that brine drainage occurred at
336 the Brussels site between 1 and 6 October (Ra >10) and between 11 and 16 October
337 (6<Ra<7) which is also confirmed by vertical nutrient distribution in the sea ice
338 [*Brabant* 2012]. At the Liège site, thicker snow muted thermal fluctuations within
339 the sea ice reducing the magnitude of changes in brine volume and salinity. Hence,
340 the variations in brine salinity and in the resulting density gradient were more
341 moderate at Liège (Figure 4), resulting in a lower Ra [*Brabant* 2012]. It is also
342 possible that some natural intra-site variability within the sea ice existed at the two
343 sampling locations. Given the textural evidence of dynamic processes at Liège [*Lewis*
344 *et al.,* 2011] one might intuit that variation within salinity especially would be
345 greater at that location but it was not observed. *Lewis et al.,* [2011] suggested that
346 snow thickness was a key component in regulating the heat fluxes and
347 morphological changes in the sea ice during our study. The ice at the Brussels site
348 had little snow accumulation (Figure 2) and larger temperature changes than the
349 Liège site (Figure 4) where the snow cover was thicker and insulated the underlying
350 sea ice cover. Indeed, snow has a low thermal conductivity, about an order of
351 magnitude lower than that of sea ice, and therefore acts as a thermal insulator
352 [*Massom et al.,* 2001].

The presence of a thick snow cover also provided overburden that resulted in negative freeboard (Figure 2). The negative freeboard observed at the Liège site toward the end of our study, associated with a permeable sea ice cover with an interconnected brine network, caused flooding of the ice surface and formed a saline slush layer [*Lewis et al.,* 2011]. Nutrient distribution data in the sea ice further confirmed that flooding occurred [*Brabant* 2012].

b. Physical controls on inorganic carbon in sea ice

Larger sea ice temperatures changes observed at the Brussels site were associated with generally higher brine salinities (Figure 4 and 5), higher TA, TCO_2, and *in situ* pCO_2 and lower pH_T (Figure 5) compared to the Liège site. These differences were expected because most solute concentrations increase with brine salinity, which also decreases CO_2 solubility [*Papadimitriou et al.,* 2004]. As the temperature changes were mainly observed in the upper layer of the ice cover, the differences in salinity, TA, pH_T, TCO_2 and pCO_2 between the upper and lower brine samples were greater at Brussels than at Liège (Figure 5). However, it is surmised that vertical redistribution of brine between 1 and 6 October homogenized brine salinity, TA, pH_T, TCO_2 and pCO_2 between the two-sackhole depths sampled on 6 October. Sea ice temperature decreased between 11 and 16 October increasing the upper brine salinity and TA (Figure 5) while the brine volume shrank below the 5% level (Figure 4), which in theory should indicate impermeability of the sea ice [*Golden et al.,* 2007] at that thickness, isolating the upper brine layer from those below. Therefore, large differences were observed in salinity, TA, TCO_2 and pH_T between the upper layer and lower brine samples. At Liège, thermal fluctuations in

376 the ice cover were limited by thicker snow cover, resulting in small differences in
377 salinity, TA, pH_T, TCO_2 and *in situ* pCO_2 between the upper and lower brine sample
378 depths (Figure 5).

379 Brine pCO_2 and, to a lesser extent, bulk ice pCO_2 both seem to follow the
380 observed cyclical variations in the ice temperatures (Figure 6) indicating that the
381 dilution – concentration effect in large part controls the pCO_2. As the ice cover cooled
382 the pCO_2 increased slightly (*e.g.*, on 6, 16 October at the Brussels site and on 18
383 October at the Liège site; Figures 4 and 5). Conversely, pCO_2 dropped as
384 temperatures rose (*e.g.*, on 11 and 21 October at Brussels and on 23 October at
385 Liège). Because pCO_2 is highly dependent on temperature, the changes in both brine
386 and bulk ice pCO_2 were larger at the Brussels site than at the Liège site (due to the
387 increased insulation provided by the snow cover in the latter). In addition, greater
388 changes in brine volume content throughout the ice column at the Brussels site
389 (Figure 4) led to more variability in brine pCO_2 than in the bulk ice due to the effects
390 of brine dilution – concentration (Figure 6). At the Liège site, the pCO_2 variations
391 were limited by small variations in ice temperature under the thicker snow cover
392 (Figure 4). Surface flooding on 18 and 23 October, might have hydrostatically forced
393 high pCO_2 seawater laterally or upward through the ice matrix. An increase of the *in*
394 *situ* brine pCO_2 and TA was observed on 18 October but these parameters decreased
395 on 23 October (Figure 5-6). Therefore, the TA and pCO_2 fluctuations observed
396 between the 18 and 23 October could also be solely explained by the changes in the
397 thermal regime (cooling and then warming). Brine salinity seems to be the main
398 control on the brine carbonate system; both *n*TA and $nTCO_2$ from both stations were

399 relatively constant through most of the sampling period. The small scatter in the
400 $nTCO_2$ concentrations could simply be due to errors in calculating $nTCO_2$ from TA
401 and pH_T. Further, the general agreement between the measured and calculated brine
402 pCO_2 values (Figure 5) seems to support the assumption that the equilibrium
403 constants are valid at subzero temperatures and high salinities [*Marion* 2001; *Delille*
404 *et al.,* 2007]. Only on 1 October did the measured and calculated brine pCO_2 values
405 differ substantially, possibly because of errors in any of the measured parameters on
406 that first day of sampling.

407 The *in situ* brine pCO_2 values are more variable than those in bulk ice (Figure 6).
408 Sampling brine using the sackhole technique provides the advantage of a direct *in*
409 *situ* measurement, but the origin of the brine that collects in the sackhole is
410 unknown, and only brine that can move easily within the ice matrix is sampled. In
411 addition, sackholes are subject to air-sea exchange during sampling, so the low pCO_2
412 brine could well have absorbed at least some CO_2 from the air above it before we
413 completed our measurements. Brine collected using the sackhole technique
414 represents interconnected liquid brine inclusions, in the form of relatively large
415 brine channels susceptible to mixing with the underlying, high pCO_2 seawater due to
416 the flooding or other types of vertical redistribution. In comparison, our bulk ice
417 pCO_2 analyses address brine at a well-defined location within the sea ice and include
418 both brines and gas bubbles trapped within the ice matrix. It should be stressed that
419 small isolated brine pockets trapped and isolated in the ice matrix are not sampled
420 using the sackhole technique but are nevertheless included in the bulk ice pCO_2
421 measurement. On the other hand, the relatively small size of the bulk ice pCO_2

sample (4 x 4 x 4.5 cm) might result in not including a (fast responding) brine channel, the latter typically being several centimeters apart. Therefore, changes in bulk ice pCO_2 values are less variable, reflecting mostly internal melting due to temperature and resultant salinity changes in the ice cover. Sackhole brines samples highlight rapid changes in the brine network such as a cooling/warming events in the ice, input of high pCO_2 seawater or from brine convection and possible contamination from contact with the atmosphere during the 10-60 minute collection time window.

c. Biological controls on carbon dynamics within sea ice

Dumont [2009] and *Brabant* [2012] presented a complete description of the distribution and concentration of organic matter, including chlorophyll-*a* (e.g. Figure 9) in sea ice at both the Brussels and Liège sites. The vertical Chl *a* distributions were more variable at Liège site than at Brussels, but at neither site showed clear variations in Chl *a* associated with the changes in pCO_2, save for during the flooding event at Liège from 18 to 23 October, which increased Chl *a* and pCO_2. However, the presence of biology may overall contribute to the low pCO2 measured on both sea ice and brine samples. The persistent opposite trends of the Chl *a* and pCO_2 profiles at Liège might reflect this contribution.

d. Antarctic sea ice as a spring-time sink of atmospheric CO_2 – comparison with the Arctic.

The bulk ice pCO_2 values observed during the present study in the Antarctic are within the same range as those few records existing in the Arctic at Barrow, Alaska

444 [*Geilfus et al.,* 2012b], and Resolute Bay, Canada [*Geilfus et al.,* 2014] (Figure 10),
445 where sampling also included melting, nearly isothermal first-year landfast sea ice in
446 late spring. Higher pCO_2 values were reported from early spring sea ice at Barrow
447 [*Geilfus et al.,* 2012b] and from SW Greenland [*Crabeck et al.,* 2014]. Although based
448 on limited data, Antarctic sea ice may have lower pCO_2 values than Arctic sea ice at
449 the same ice temperature (Figure 10), although differences in the sea ice texture and
450 dynamical forcing between the two poles are important and may have substantial
451 effects on permeability (and therefore fluxes) and should be further investigated. It
452 is noteworthy that the observed range of concentrations suggests that Antarctic sea
453 ice becomes undersaturated in CO_2 relative to the atmosphere early in the winter–
454 spring transition and reaches levels not observed in Arctic sea ice until much later in
455 the spring decay process [*Geilfus et al.,* 2012a,b; 2014; *Crabeck et al.,* 2014].

456 The bulk ice pCO_2 data were collected at different times of the year in the Arctic
457 and in the Antarctic (early to late spring) under different temperature and salinity
458 conditions. Therefore we looked at the relationship between the bulk ice pCO_2 and
459 the brine volume (Figure 10c). At low brine volumes (due to low T and/or high S)
460 the bulk ice pCO_2 is high while at high brine volumes (due to high T and/or low S)
461 the bulk ice pCO_2 is low (Figure 10c). It should also be noted that both in the Arctic
462 and in the Antarctic, spring sea ice can become undersaturated in CO_2 while the
463 underlying seawater is supersaturated with respect to the atmosphere (Figure 7)
464 [*Papakyriakou and Miller,* 2011].

465 During this study, we observed a net uptake of atmospheric CO_2 by the snow and
466 sea ice at both sites. This uptake was in the same order of magnitude as previous

fluxes reported over Antarctic sea ice during the austral summer by *Delille* [2006] and *Nomura et al.,* [2013] and over Arctic sea ice by *Semiletov et al.,* [2004], *Nomura et al.,* [2010a,b], and *Geilfus et al.,* [2012a; 2013; 2014], using similar chamber techniques. At the Brussels site, fluxes measured over snow were similar to those measured over bare ice suggesting the thin snow cover had a limited impact on CO_2 exchange between the atmosphere and sea ice. At the Liège site, thicker snow cover reduced the magnitude of the fluxes. The snow cover could have acted as a buffer between the ice and the atmosphere, as suggested by *Miller et al.,* [2011]. However, in contrast to *Nomura et al.,* [2010b], a snow cover thicker than 9 cm did not seem to completely prevent the CO_2 exchanges between the ice and the atmosphere.

6. Conclusions

The inorganic carbon dynamic within sea ice responds swiftly to short-term meteorological events during the SIMA expedition. The succession of warm and cold events impacted the physical properties of the sea ice and its inorganic carbon dynamics. Snow thickness modulated the heat flux to the sea ice, which impacted its salinity and therefore the sea ice carbonate system. Less snow and larger temperature variations created larger variations in brine salinity, TA, TCO_2, and brine and bulk ice pCO_2. In addition, the combination of unstable salinity gradients within the ice cover and episodic warming events initiated vertical brine redistribution at the low-snow site on two occasions homogenizing brine properties vertically. At the end of the survey, flooding occurred due to snow loading at the Liège site, bringing high pCO_2 seawater into the brine system.

During the early spring, sea ice was undersaturated and largely controlled by the brine dilution, although a potential impact of biology could contribute to the overall undersaturation. We highlighted contrasted pCO_2 dynamics in bulk ice measurements as compared to sackholes measurements. The bulk ice pCO_2 values were much less variable, reflecting mostly internal temperature and salinity driven thermodynamic changes while pCO_2 variations in sackhole brine reflected rapid transport within an interconnected brine channel network as well as potential exchange with the atmosphere and underlying surface waters.

At both sampling sites, the ice cover acted as a sink for atmospheric CO_2, even despite episodic flooding by supersaturated seawater. Thus, during early spring the inorganic carbonate system in the sea ice of the Bellingshausen Sea behaved as a transition layer between the ocean and the atmosphere, reacting to atmospheric forcing and from episodic interactions with the seawater.

7. Acknowledgments

The authors are grateful to the officers and crew of the RVIB *Nathaniel B. Palmer* for their logistical assistance during the SIMBA cruise. We thank Kristel De Potter for helping with measuring the bulk ice pCO_2 and Keith Johnson for his help during sample collection. The SIMBA project was supported by the National Science Foundation under NSF Grant ANT 0703682 – Sea Ice Mass Balance in the Antarctic to UTSA (S.F. Ackley, PI). This work was carried out within the framework of the Belgian research program Action de Recherche Concertée “Sea Ice Biogeochemistry in a CLIMate change perspective” (ARC-SIBCLIM) financed by the Belgian French Community under contract n° ARC-02/7-318287, the BELCANTO project (contracts

SD/CA/03A&B) financed by the Belgian Federal Science Policy Office, and the Fonds de la Recherche Scientifique – FNRS (FRFC 2.4649.07). N.-X. Geilfus was supported by a FRIA (Fonds pour la Recherche en Industrie Agronomiques) grant and a grant from the Arctic Research Center, Aarhus University. S. Rysgaard acknowledges the Canada Excellence Research Chair Program. B. Delille is a research associate of the Fonds de la Recherche Scientifique – FNRS. This is a Mare contribution and a contribution to the Arctic Science Partnership (ASP), www.asp-net.org.

8. Bibliography

Brabant, F. (2012), Physical and biogeochemical controls on the DMS/P/O cycle in Antarctic sea ice, pp. 300 pp, Universite Libre de Bruxelles, Bruxelles.

Copin Montégut, C. (1988), A new formula for the effect of temperature on the partial pressure of carbon dioxide in seawater, *Marine Chemistry*, *25*, 29-37.

Cox, G. F. N., and W. F. Weeks (1983), Equations for determining the gas and brine volumes in sea-ice samples, *Journal of Glaciology*, *29*(102), 306 - 316.

Crabeck, O., B. Delille, D. N. Thomas, N. X. Geilfus, S. Rysgaard, and J. L. Tison (2014), CO2 and CH4 in sea ice from subarctic fjord, *Biogeosciences Discuss.*, *11*, 4047-4083.

Delille, B. (2006), Inorganic carbon dynamics and air-ice-sea CO_2 fluxes in the open and coastal waters of the Southern Ocean, 296 pp, Université de Liège, Liège.

Delille, B., B. Jourdain, A. V. Borges, J. L. Tison, and D. Delille (2007), Biogas (CO_2, O-2, dimethylsulfide) dynamics in spring Antarctic fast ice, *Limnology and Oceanography*, *52*(4), 1367-1379.

Delille, B., M. Vancoppenolle, N.X. Geilfus, B. Tilbrook, D. Lannuzel, V. Schoemann, S. Becquevort, G. Carnat, D. Delille, C. lancelot, L. Chou, G.S. Dieckmann, J.-L. Tison (2014). Southern Ocean CO_2 sink: the contribution of the sea ice , *Journal of Geophysical Research-Oceans*, 119, doi:10.1002/2014JC009941.

Dickson, A. G., and F. J. Millero (1987), A comparison of the equilibrium constants for the dissociation of carbonic acid in seawater media, *Deep Sea Research*, *I*(34), 1733-1743.

Dieckmann, G. S., and H. H. Hellmer (2010), The importance of Sea Ice: An Overview, in *Sea Ice, second edition*, edited by D. N. Thomas and G. S. Dieckmann, pp. 1-22, Wiley- Blackwell, Oxford.

DOE (Ed.) (1994), *Handbook of methods for the analysis of the various parameters of the carbon dioxide system in sea water*, version 2, edited by Dickson, A. G. and Goyet, C., ORNL/CDIAC-74.

Dumont, I. (2009), Interactions between the microbial network and the organic matter in the Southern Ocean: impacts on the biological carbon pump, 202 pp, Université Libre de Bruxelles, Bruxelles.

Eicken, H. (1992), Salinity Profiles of Antarctic Sea Ice - Field Data and Model Results, *Journal of Geophysical Research-Oceans*, *97*(C10), 15545-15557.

Frankignoulle, M. (1988), Field-Measurements of Air Sea CO_2 Exchange, *Limnology and Oceanography*, *33*(3), 313-322.

Frankignoulle, M., and A. V. Borges (2001), Direct and indirect pCO_2 measurements in a wide range of pCO_2 and salinity values (the Scheldt estuary), *Aquatic Geochemistry*, *7*(4), 267-273.

Geilfus, N. X., G. Carnat, T. Papakyriakou, J. L. Tison, B. Else, H. Thomas, E. Shadwick, and B. Delille (2012a), Dynamics of pCO(2) and related air-ice CO2 fluxes in the Arctic coastal zone (Amundsen Gulf, Beaufort Sea), *Journal of Geophysical Research-Oceans*, *117*, C00G10, doi:10.1029/2011JC007118.

Geilfus, N. X., B. Delille, V. Verbeke, and J. L. Tison (2012b), Towards a method for high vertical resolution measurements of the partial pressure of CO2 within bulk sea ice, *Journal of Glaciology*, *58*(208), 287-300.

Geilfus, N. X., G. Carnat, G. S. Dieckmann, N. Halden, G. Nehrke, T. Papakyriakou, J. L. Tison, and B. Delille (2013), First estimates of the contribution of $CaCO_3$ precipitation to the release of CO_2 to the atmosphere during young sea ice growth, *Journal of Geophysical Research*, *118*, 224-255, doi:10.1029/2012JC007980.

Geilfus, N. X., R. J. Galley, O. Crabeck, T. Papakyriakou, J. C. Landy, J. L. Tison, and S. Rysgaard (2014), Inorganic carbon dynamics of melt pond-covered first year sea ice in the Canadian Arctic, *Biogeosciences Discuss.*

Gleitz, M., M. R. vd Loeff, D. N. Thomas, G. S. Dieckmann, and F. J. Millero (1995), Comparison of summer and winter inorganic carbon, oxygen and nutrient concentrations in Antarctic sea ice brine, *Marine Chemistry*, *51*(2), 81-91.

Golden, K. M., S. F. Ackley, and V. I. Lytle (1998), The percolation phase transition in sea ice, *Science*, *282*(5397), 2238-2241.

Golden, K. M., H. Eicken, A. L. Heaton, J. Miner, D. J. Pringle, and J. Zhu (2007), Thermal evolution of permeability and microstructure in sea ice, *Geophysical Research Letters*, *34*(16), L16501, doi:10.1029/2007GL030447.

578 Gran, G. (1952), Determination of the equivalence point in potentiometric titration,
579 *Analyst*, *Part II*(77), 661-671.

580 Leppäranta, M., and T. Manninen (1988), The brine and gas content of sea ice with
581 attention to low salinities and high temperatures, *Rep.*, Finnish Institute of Marine
582 Research, Helsinki, 15 pp.

583 Lewis, M. J., J. L. Tison, B. Weissling, B. Delille, S. F. Ackley, F. Brabant, and H. Xie
584 (2011), Sea ice and snow cover characteristics during the winter-spring transition in
585 the Bellingshausen Sea: An overview of SIMBA 2007, *Deep-Sea Research Part Ii-*
586 *Topical Studies in Oceanography*, *58*(9-10), 1019-1038.

587 Marion, G. M. (2001), Carbonate mineral solubility at low temperatures in the Na-K-
588 Mg-Ca-H-Cl-SO_4-OH-HCO_3-CO_3-CO_2-H_2O system, *Geochimica Et Cosmochimica Acta*,
589 *65*(12), 1883-1896.

590 Massom, R. A., R. A., Eicken, H., Haas, C., Jeffries, M. O., Drinkwater, M. R., Sturm, M.,
591 Worby, A. P., Wu, X., Lytle, V. I., Ushio, S., Morris, K., Reid, P. A., Warren, S. G., and
592 Allison, I.(2001), Snow on Antarctic Sea ice, *Rev. Geophys.*, *39*(3), 413-445.

593 Mehrbach, C., C. H. Culberson, J. E. Hawley, and R. M. Pytkowicz (1973),
594 Measurements of the apparent dissociation constants of carbonic acid in seawater at
595 atmospheric pressure, *Limnology and Oceanography*, *18*, 897-907.

596 Miller, L. A., M. Chierici, T. Johannessen, T. T. Noji, F. Rey, and I. Skjelvan (1999),
597 Seasonal dissolved inorganic carbon variations in the Greenland Sea and
598 implications for atmospheric CO_2 exchange, *Deep-Sea Research Part Ii-Topical Studies*
599 *in Oceanography*, *46*(6-7), 1473-1496.

600 Miller, L. A., T. Papakyriakou, R. E. Collins, J. Deming, J. Ehn, R. W. Macdonald, A.
601 Mucci, O. Owens, M. Raudsepp, and N. Sutherland (2011), Carbon Dynamics in Sea
602 Ice: A Winter Flux Time Series, *Journal of Geophysical Research-Oceans*, *116*(C02028),
603 doi:10.1029/2009JC006058.

604 Nomura, D., H. Eicken, R. Gradinger, and K. Shirasawa (2010a), Rapid physically
605 driven inversion of the air-sea ice CO_2 flux in the seasonal landfast ice off Barrow,
606 Alaska after onset surface melt, *Continental Shelf Research*, *30*(19), 1998-2004.

607 Nomura, D., H. Yoshikawa-Inoue, T. Toyota, and K. Shirasawa (2010b), Effects of
608 snow, snow-melting and re-freezing processes on air-sea ice CO_2 flux, *Journal of*
609 *Glaciology*, *56*(196), 262-270.

610 Nomura, D., M. A. Granskog, P. Assmy, D. Simizu, and G. Hashida (2013), Arctic and
611 Antarctic sea ice acts as a sink for atmospheric CO_2 during periods of snowmelt and
612 surface flooding, *Journal of Geophysical Research: Oceans*, 118, 6511-6524,
613 doi:10.1002/2013JC009048.

614 Papadimitriou, S., H. Kennedy, G. Kattner, G. S. Dieckmann, and D. N. Thomas (2004),
615 Experimental evidence for carbonate precipitation and CO_2 degassing during sea ice
616 formation, *Geochimica et Cosmochimica Acta*, *68*(8), 1749-1761.

617 Papadimitriou, S., D. N. Thomas, H. Kennedy, C. Haas, H. Kuosa, A. Krell, and G. S.
618 Dieckmann (2007), Biogeochemical composition of natural sea ice brines from the
619 Weddell Sea during early austral summer, *Limnology and Oceanography*, *52*(5),
620 1809-1823.

621 Papakyriakou, T., and L. Miller (2011), Springtime CO_2 exchange over seasonal sea
622 ice in the Canadian Arctic Archipelago, *Annals of Glaciology*, *52*(57), 215-224,
623 doi:10.3189/172756411795931533 4.

624 Parmentier, F.-J. W., T. R. Christensen, L. L. Sørensen, S. Rysgaard, A. D. McGuire, P. A.
625 Miller, and D. A. Walker (2013), The impact of lower sea-ice extent on Arctic
626 greenhouse-gas exchange, *Nature climate change*, 3, 195-202,
627 doi:10.1038/nclimate1784.

628 Rysgaard, S., R. N. Glud, M. K. Sejr, J. Bendtsen, and P. B. Christensen (2007),
629 Inorganic carbon transport during sea ice growth and decay: A carbon pump in polar
630 seas, *Journal of Geophysical Research-Oceans*, *112*(C3), C03016,
631 doi:10.1029/2006JC003572.

632 Rysgaard, S., R. N. Glud, K. Lennert, M. Cooper, N. Halden, R. J. G. Leakey, F. C.
633 Hawthorne, and D. Barber (2012), Ikaite crystals in melting sea ice – implications for
634 pCO2 and pH levels in Arctic surface waters, *The Cryosphere*, *6*, 1-8.

635 Rysgaard, S., J. Bendtsen, B. Delille, G. S. Dieckmann, R. N. Glud, H. Kennedy, J.
636 Mortensen, S. Papadimitriou, D. N. Thomas, and J. L. Tison (2011), Sea ice
637 contribution to the air-sea CO(2) exchange in the Arctic and Southern Oceans, *Tellus*
638 *Series B-Chemical and Physical Meteorology*, *63*(5), 823-830.

639 Rysgaard, S., F. Wang, R. J. Galley, R. Grimm, D. Notz, M. Lemes, N. X. Geilfus, A.
640 Chaulk, A. A. Hare, O. Crabeck, B. G. T. Else, K. Campbell, L. L. Sørensen, J. Sievers, and
641 T. Papakyriakou (2014), Temporal dynamics of ikaite in experimental sea ice, The
642 Cryosphere, 8(4), 1469-1478, doi: 10.5194/tc-8-1469-2014

643 Semiletov, I. P., A. Makshtas, S. I. Akasofu, and E. L. Andreas (2004), Atmospheric CO_2
644 balance: The role of Arctic sea ice, *Geophysical Research Letters*, *31*(5), L05121,
645 doi:10.1029/2003GL017996.

646 Thomas, D. N., and G. S. Dieckmann (2010), Sea Ice - An introduction to its physics,
647 biology, chemistry and geology, in *Sea Ice*, edited by Thomas, D. N. and Dieckmann, G.
648 S., 2nd Edn., Science, Oxford, UK, Wiley, Blackwell, p. 621, London.

649 Tison, J. L., A. Worby, B. Delille, F. Brabant, S. Papadimitriou, D. Thomas, J. de Jong, D.
650 Lannuzel, and C. Haas (2008), Temporal evolution of decaying summer first-year sea

ice in the Western Weddell Sea, Antarctica, *Deep-Sea Research Part Ii-Topical Studies in Oceanography*, *55*(8-9), 975-987.

Vancoppenolle, M., Timmermann, R., Ackley, S. F., Fichefet, T., Goosse, H., Leonard, K. C., Lieser, J., Nicolaus, M., Papakyriakou, T., and Tison, J.-L.: Assessment of radiation forcing data sets for large-scale sea ice models in the Southern Ocean, Deep-Sea Res. Pt. II, 58, 1237–1249, 2011.

Weeks, W. F. (Ed.): On Sea Ice, Fairbanks, University of Alaska Press, Alaska, 664 pp., 2010.

Zemmelink, H. J., Delille, B., Tison, J. L., Hintsa, E. J., Houghton, L., and Dacey, J. W. H.: CO2 deposition over the multi-year ice of the western Weddell Sea, Geophys. Res. Lett., 33, L13606, doi:10.1029/2006GL026320, 2006.

9. Figure captions

Figure 1: Location of the sampling area for the SIMBA cruise 2007 (blue patch), in the Bellingshausen Sea, Antarctica.

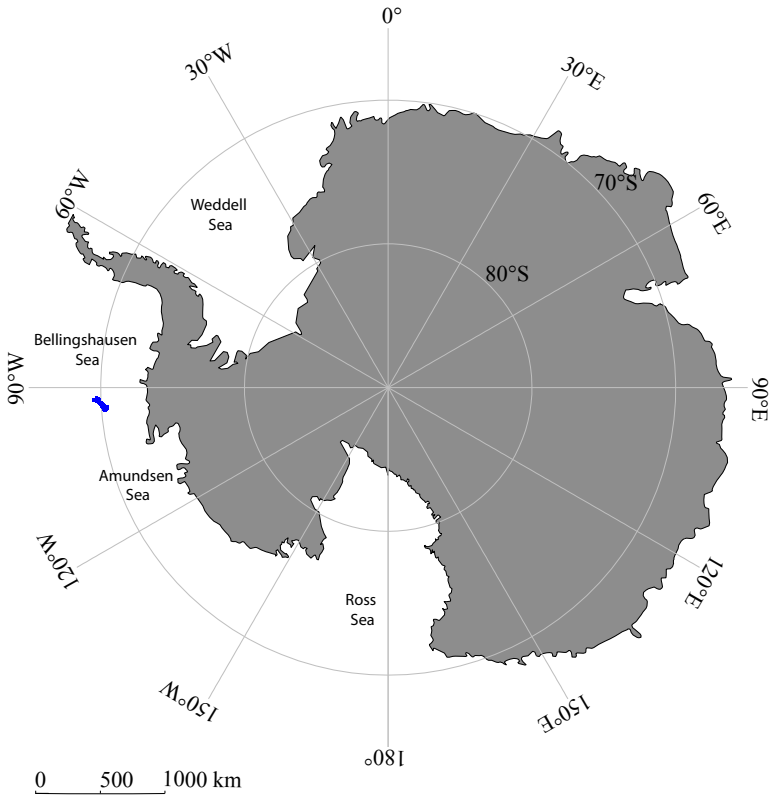

Figure 2: Ice (including range of observed values), snow thickness and freeboard at the Brussels and Liège sites.

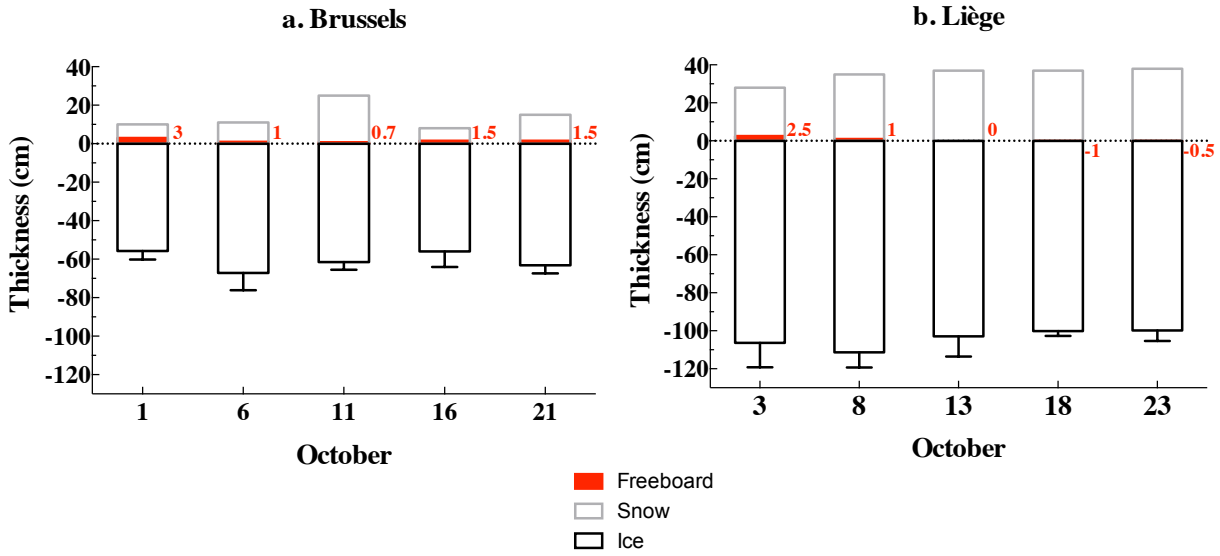

Figure 3: Daily time series of air temperature (°C) recorded on the ship and the surface ice temperature of the different sampling stations at Brussels (red dots) and Liège (blue dots) site.

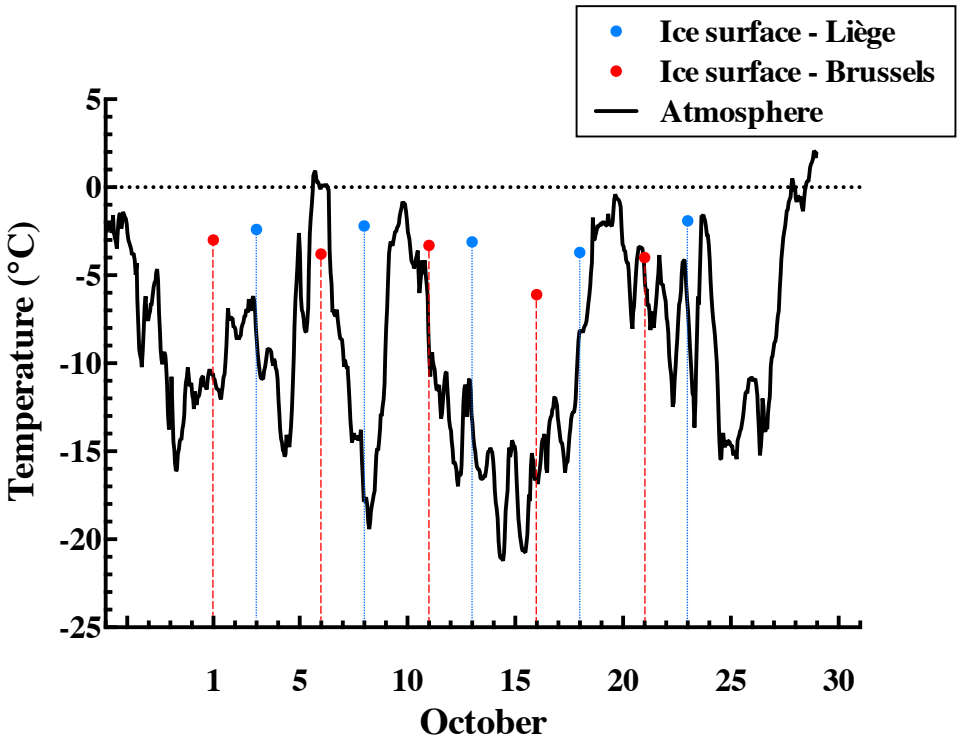

683 Figure 4: Profiles of temperature (°C), bulk ice salinity, calculated brine salinity,
684 brine volume fraction, and ^{18}O isotopic ratio from the Brussels (top) and
685 Liège (bottom) sites.
686

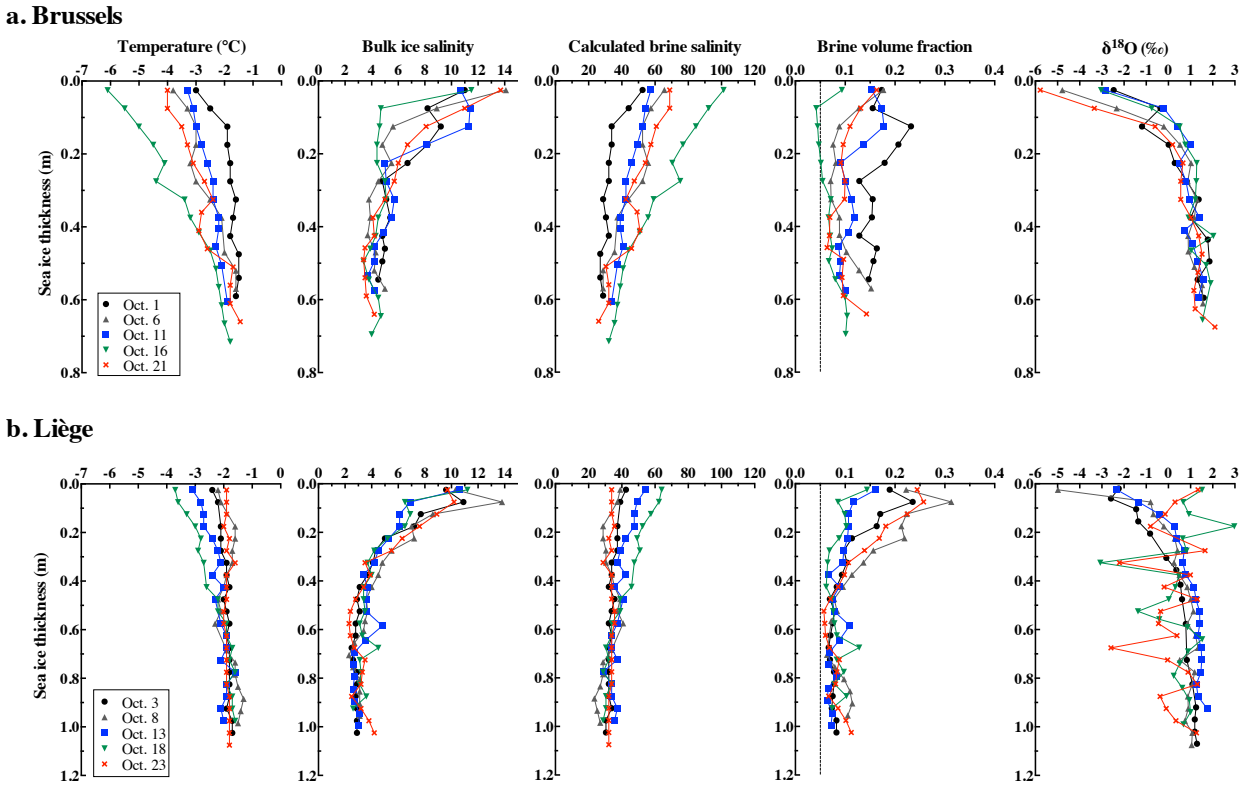

687
688
689

Figure 5: Evolution of salinity, pH_T, TA (in µmol kg^{-1}), *n*TA (TA normalized to a salinity of 34, in µmol kg^{-1}), calculated TCO_2 (in µmol kg^{-1}) and $nTCO_2$ (TCO_2 normalized to a salinity of 34, in µmol kg^{-1}), measured and calculated pCO_2 (in µatm) in surface and deep brine sackholes from the Brussels (Bxl) and Liège (Lg) sites. The dotted line represents the atmospheric pCO_2 in October 2007.

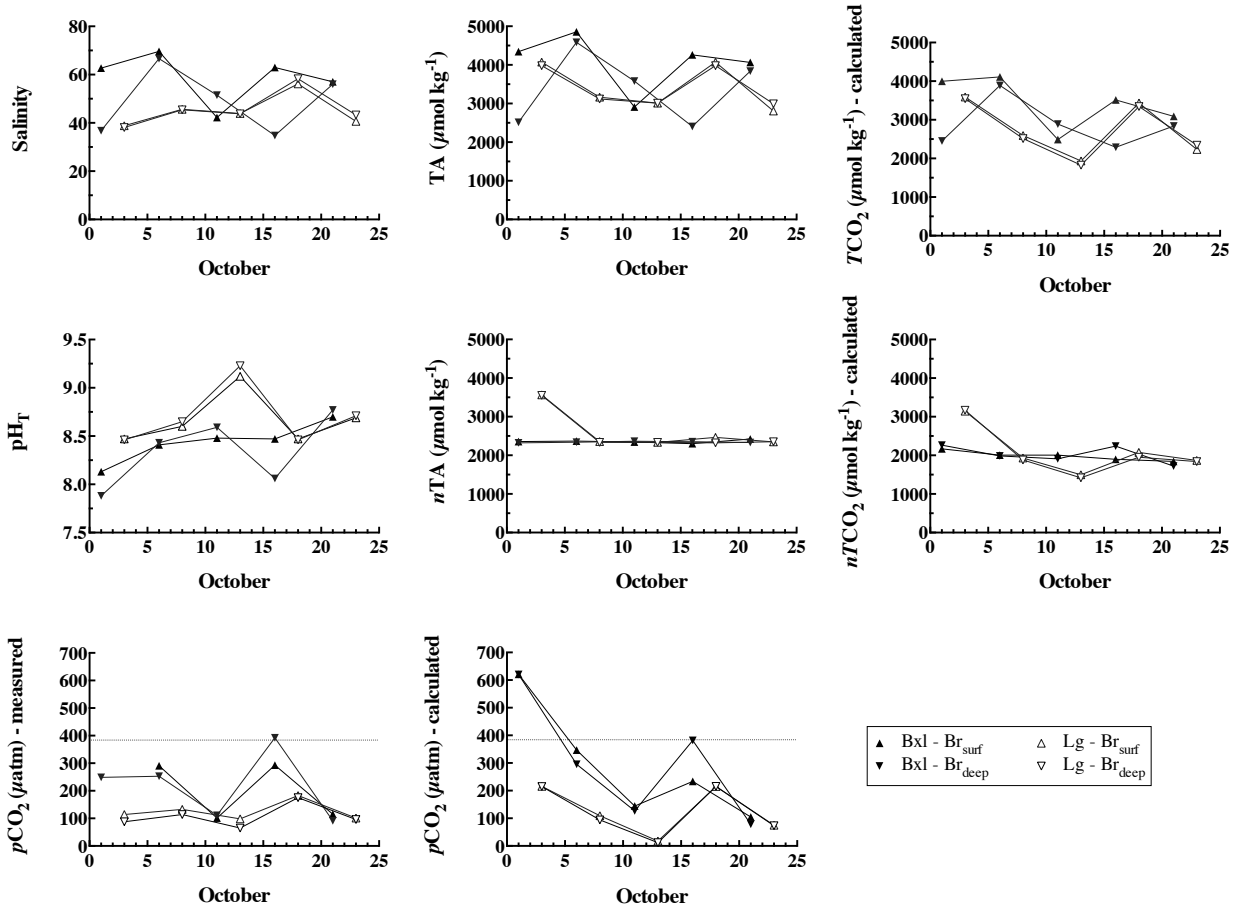

Figure 6: Vertical profiles of the *in situ* brine pCO_2 (in µatm) and bulk ice pCO_2 (in µatm) from the Brussels (top) and Liège (bottom) sites.

Data at 0.075 – 0.125 and 0.175 m depth of the station on 16 October were measured while the brine volume was 4.1 – 4.4 and 4.6 %, respectively.

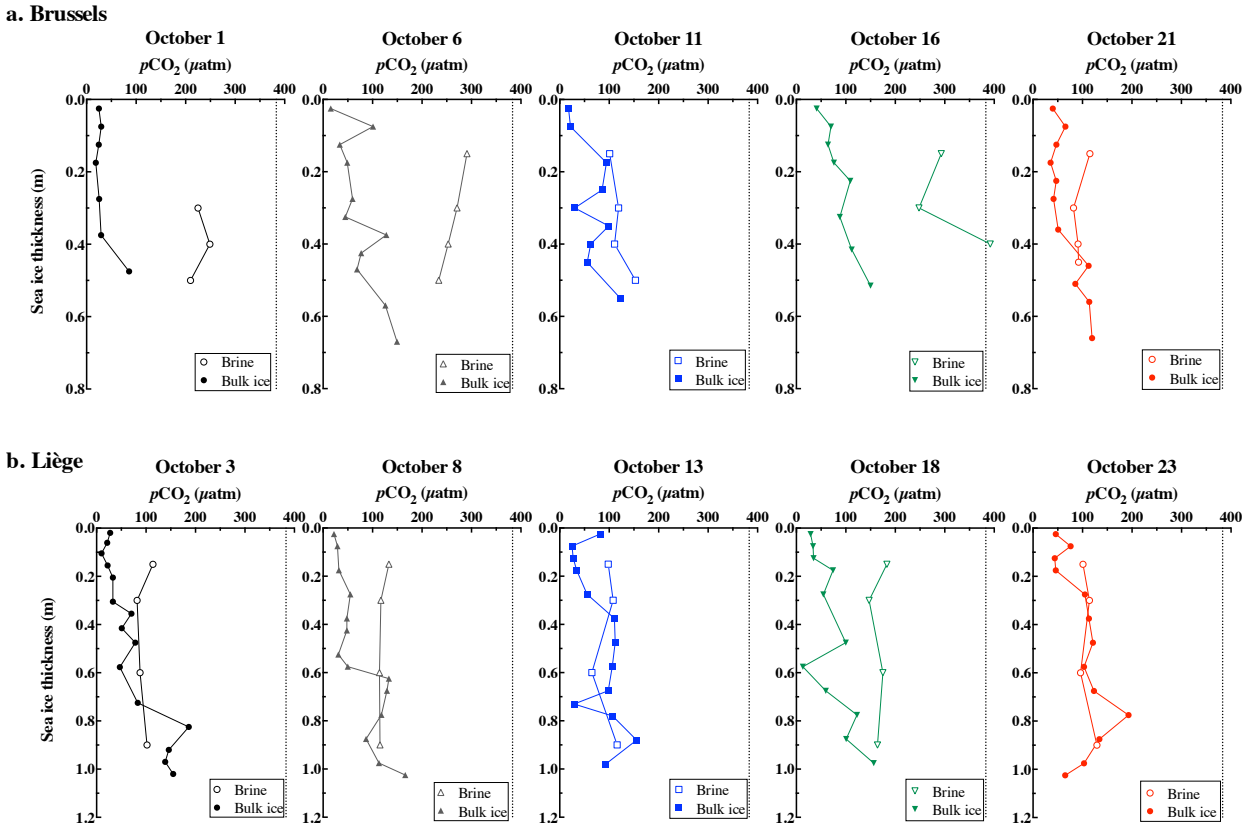

Figure 7: Evolution of salinity, pH_T, TA (in µmol kg^{-1}), *n*TA (TA normalized to a salinity of 34, in µmol kg^{-1}), calculated TCO_2 (in µmol kg^{-1}) and $nTCO_2$ (TCO_2 normalized to a salinity of 34, in µmol kg^{-1}), *in situ* pCO_2 (in µatm) in the underlying seawater at the ice-water interface and 1 and 27m below the ice-water interface. The dotted line represents the atmospheric pCO_2 in 2007.

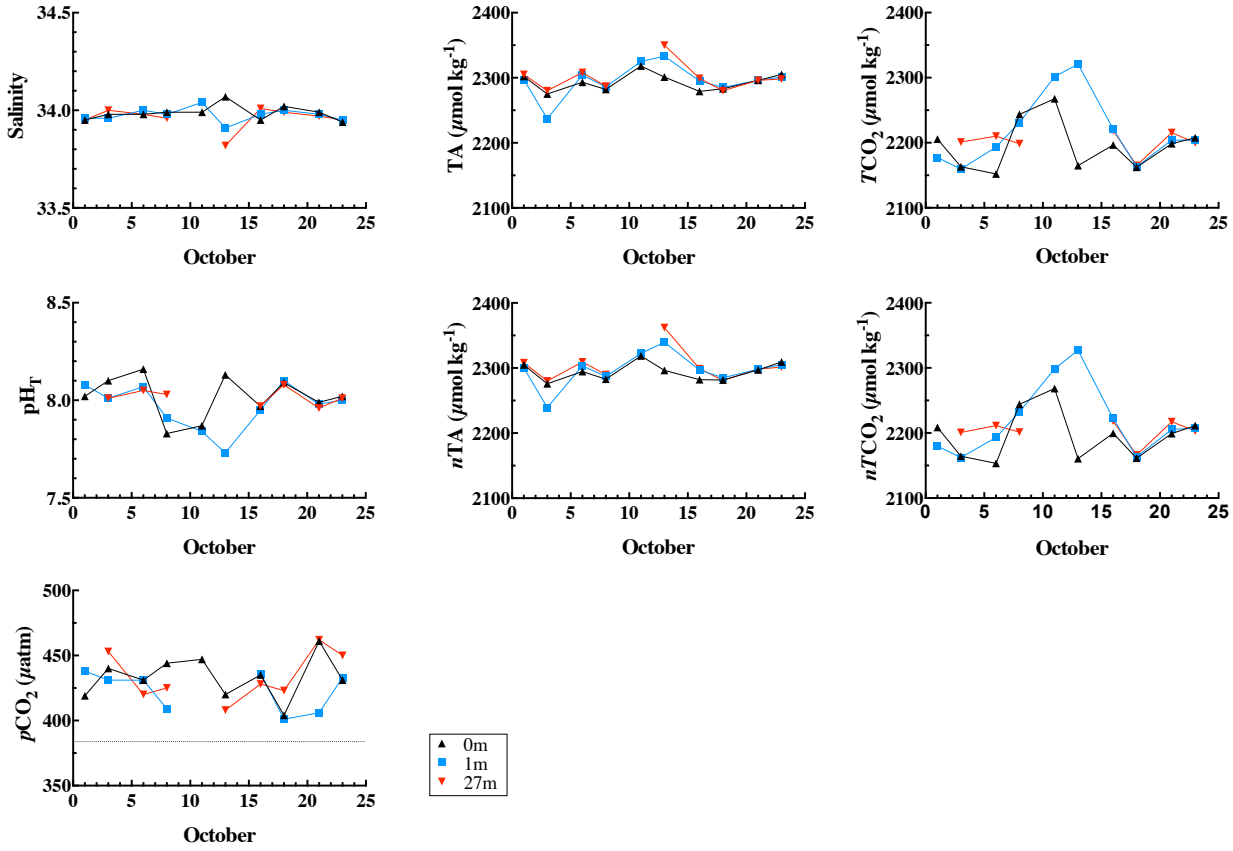

718 Figure 8: CO_2 fluxes (in mmol m^{-2} d^{-1}) measured over sea ice and snow for the

719 Brussels and Liège sites.

720

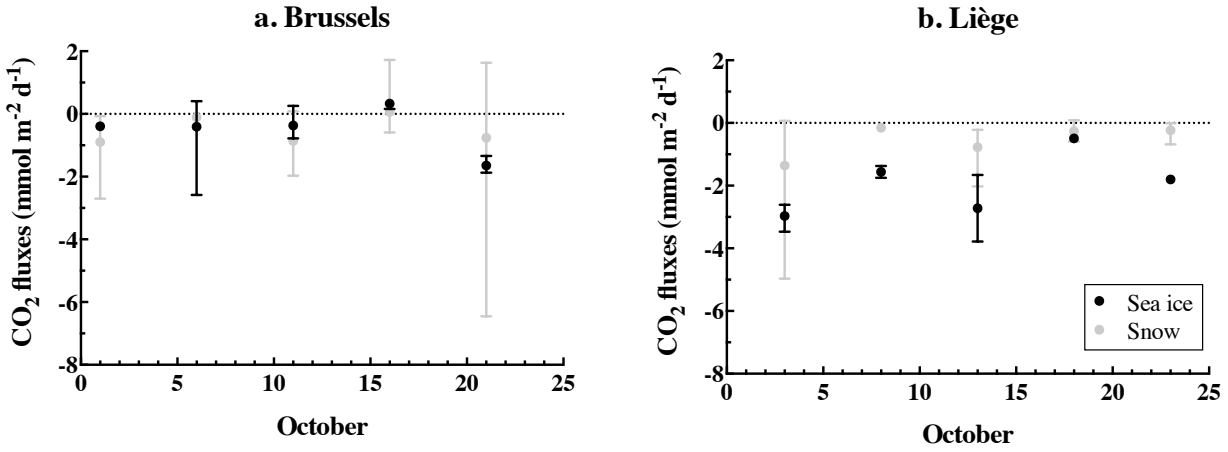

721

722

723

Figure 9: Profiles of Chl *a* concentration within bulk sea ice at the Brussels and Liège sites, adapted from *Dumont* [2009].

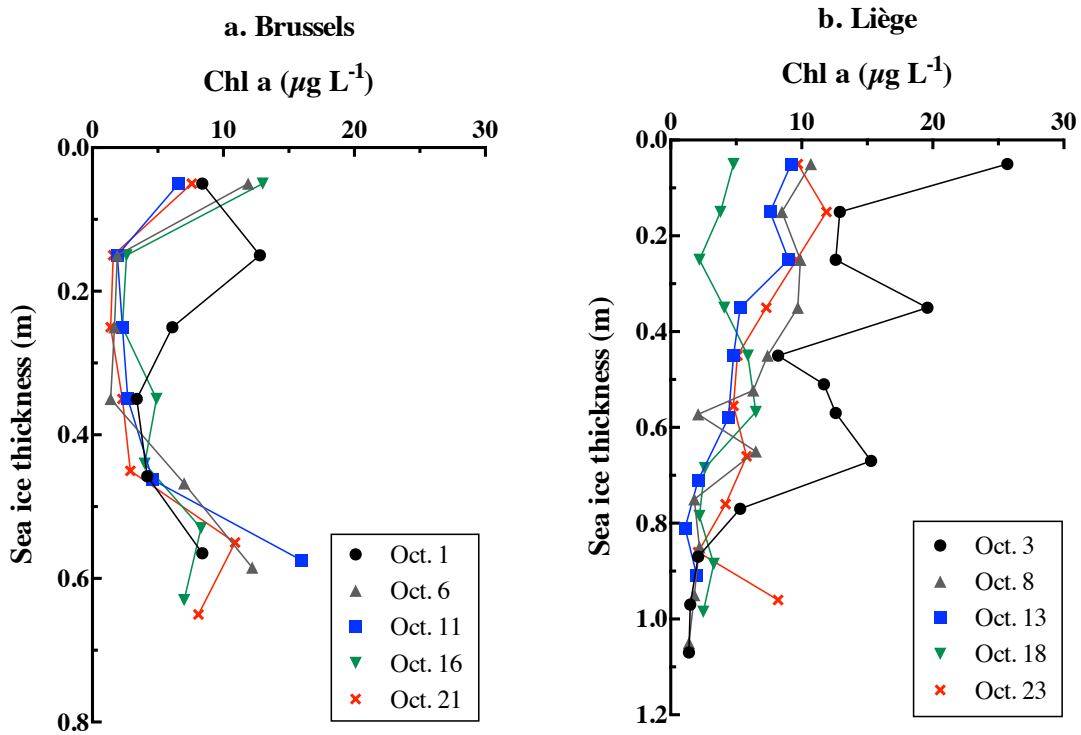

Figure 10: a) The relationships between bulk ice pCO_2 (in µatm) and temperature measured in Antarctic (this study) and Arctic (Geilfus et al., 2012b; 2014; Crabeck et al., 2014) sea ice. b) The relationships between *in situ* brine pCO_2 (in µatm) and brine temperature in the Antarctic (this study; Delille 2006; Delille et al., 2007) and Arctic sea ice (Geilfus et al., 2012a). c) Relationship between the bulk ice pCO_2 (in µatm) and the brine volume fraction (in %) measured in Antarctic (this study) and Arctic (Geilfus et al., 2012b; 2014; Crabeck et al., 2014) sea ice.